Mansoura Journal of Chemistry, vol. 34(2), December 2007

SULFATED ZIRCONIA MODIFIED PILLARED MONTMORILLONITE CATALYTIC EVALUATION IN N-HEXANE TRANSFORMATION

D. Radwan[a,*], L. Saad[a], S. Mikhail[a] and S. A. Selim [b]
[a]Egyptian Petroleum Research Institute- Refining Division,
Hai Elzohoor-Nasr City- Cairo-Egypt.
[b]Ain Shams University, Faculty of Science, El-Abasia-Cairo –Egypt.
(Received: 16 / 10 / 2007)

ABSTRACT

Sulfated zirconia pillared clay was prepared by adding the sulfate to the zirconium species before the pillaring process. The intercalated clay was then characterized by DTA, FT-IR, X-ray diffraction and N_2-adsorption. It was found that the pillaring process using sulfated zirconia as intercalating agent gave rise to good thermal stability, increase in the d-spacing of the bentonite clay from 12 to 19Å, and created a wider pore size.

The conversion of n-hexane catalyzed by the sulfated zirconia pillared clay was investigated using a flow system operating under atmospheric pressure and at a temperature range 180-300°C. Results indicated that, SZ-PILC is more active than SZ catalyst in n-hexane transformation. The major primary reaction was isomerization, giving monobranched and dibranched isomers. Small amounts of cracking, cyclic and aromatic products were also observed.

Keywords: Pillared clay; sulfated zirconia; X-ray; IR; Catalytic activity.

1. INTRODUCTION

In order to protect the environment, several sets of regulations have been established. Owing to this legislation, great interest has been devoted to the substitution of unfriendly and corrosive liquids, used in

*Corresponding author; Fax: +2022747433
Postal code: 1172 E-mail address: dalia_epri@yahoo.com

chemical and petrochemical industries by solid catalysts. On this basis, clays may constitute very promising substitutes.

When inorganic species are introduced into the interlayers of the clay, the resulting nanocomposite can be used as a catalyst for specific reactions. The intercalated species are able to prevent the collapse of the interlayer spaces giving rise to two-dimensional porous materials "pillared clay materials" **[Vaughan (1988) and Lambert & Poncelet (1997)]**.

The pillared clays are usually used as cracking catalysts because they develop a good acidity and good thermal stability. Beside the acidity of the clay layers, the metal oxide pillars also show an acidic character. However, the modification of the metal oxide pillars by electronegative ions like sulfates, results in the production of strongly acid components **[Bouchenafa-saib et al. (2004) and Issaadi et al. (2006)]**, where the inductive effect of the S=O group increases the charge in the neighbor metal cation (M^+).

Faran-Torres & Grang (1990, 1991, 1992); Katoh et al. (1994) and Ben Chaabene et al. (2002) modified the acidity of $ZrOCl_2$ montmorillonite by adding $(NH_4)_2SO_4$ during the intercalation reaction. The intercalation of zirconium sulfate hydroxyl complex in Na-montmorillonite using zirconium acetate as a precursor was also studied **[Bergaoui et al. (2002)]**.

In the present investigation, a new preparation method is applied by including an initial sulfation that creates a sulfated species in the intercalation solution. The effect of sulfate precursor on the textural properties and catalytic activity of the prepared sulfated zirconia pillared clay catalysts is studied.

2. EXPERIMENTAL

2.1 Preparation method

2.1.1. Preparation of Sulfated Zirconia (SZ) Catalyst

Ammonium sulfate was added to 0.1 mole $ZrOCl_2$ solution freshly prepared with SO_4: Zr molar ratio equal to 0.15. The solution was then subjected to reflux for 4 hours, then evaporated, washed by distilled water until free from chloride ion and dried at 120°C for 4h, followed by calcination at 450°C in the presence of purified air for 6 hours.

2.1.2. Preparation of Sulfated Zirconia Pillared clay (SZ-PILC):

The starting clay material (bentonite from Alexandria district) was dispersed in freshly prepared 1M solution of NH_4OH (10g/L) for one day, and then aged in distilled water for at least three days. The suspended part then centrifuged, washed by distilled water, and dried at room temperature. The solid sample obtained was sieved to 200 mesh.

The intercalated clay was prepared by adding the freshly refluxed sulfated zirconia solution drop wise to 10g/l clay suspensions. The slurry was refluxed for 4h, washed by distilled water and left to dry at room temperature. The sample was then calcined in a flow of purified air at 450°C and 550°C for 6h [Calc.I & Calc.II respectively].

2.2. Characterization of the prepared pillared clay:

The structure of the prepared interlayered clay samples was studied by various techniques;

Thermal analysis (DTA) was carried out in temperature range from room temperature to 1000°C (heating rate 10°C /min) on the prepared catalyst samples under a flow of Ar using SETARAM Labsys TG-DSC16 to trace the structure changes accompanying the thermal treatment.

Infrared Spectroscopic Analysis (FTIR) was carried out using ATI Mattson 1001 to characterize the main constituents of the prepared samples.

X-Ray Diffraction Analyses (XRD) were carried out by a Shimadzu XD-1 diffractometer using Cu-target Ni-filter to study the different phases of the intercalated samples that accompany the intercalation process.

The textural properties were determined from the adsorption-desorption isotherms measured at liquid nitrogen temperature using NOVA 3200e sorption, the specific surface area was evaluated by the BET method, pore size and pore volume data were obtained by the BJH method. All samples were degassed at 200°C for 17h in nitrogen atmosphere prior to adsorption.

2.3. The catalytic activity:

The catalytic transformation of n-hexane over the prepared pillared interlayer clay catalysts was performed in a flow system operated under atmospheric pressure, at the temperature range 180-300°C,

hydrogen flow rate 35ml/min, catalyst volume 5ml and liquid hourly space velocity (LHSV) 0.6 hr^{-1}.

A Perkin-Elmer gas chromatography, hydrogen flame ionization detector was used to analyze the reaction products using capillary column throughout this investigation.

3. RESULTS AND DISCUSSION

3.1 Structural Characterization

3.1.1 Thermal Analysis

Figure 1(a-c) illustrates the differential thermal analysis (DTA) profiles for SZ sample, parent bentonite clay, and the prepared SZ-PILC.

DTA profile for SZ (Fig.1-a) catalyst exhibits four endothermic features. Three of them occur below 400°C that can be identified as;
At ≈ 110°C: evolution of water molecules loosely adsorbed on the external surface.
At ≈200°C: evolution of water molecules strongly associated with hydroxyl zirconium cations **[Vera (2002)]**, and at ≈ 300°C: dehyroxylation and crystallization of bulk $Zr(OH)_4$ into ZrO_2. The fourth endothermic feature at ≈ 700°C is attributed to the loss of SO_2 **[Srinivasan et al. (1995)]**. One exothermic peak at ≈ 900°C is due to phase transformation of ZrO_2 from metastable tetragonal phase to stable monoclinic phase **[Watkins (1995)]**.

The DTA curve for the starting bentonite clay shows three main endothermic processes, the endotherm at ≈100°C corresponds to the loss of physically adsorbed water on the external surface, the presence of shoulder near to 200°C indicates that this raw material is calcium-montmorillonite type **[Barshad (1950)]**. Very small endothermic feature at ≈ 280°C was observed which may be attributed to escape of interlayer water. The higher temperature endotherm at ≈ 550°C is corresponding to the beginning of the collapse of the interlayer structure as a result of the decomposition of the silicate structure with loss of a water molecule per formula unit by dehydroxylation **[Yamanaka & Brindley (1979)]**. The exothermic peak that appears at 930°C is a structural one, which attributed to the destruction of montmorillionte and formation of new phases.

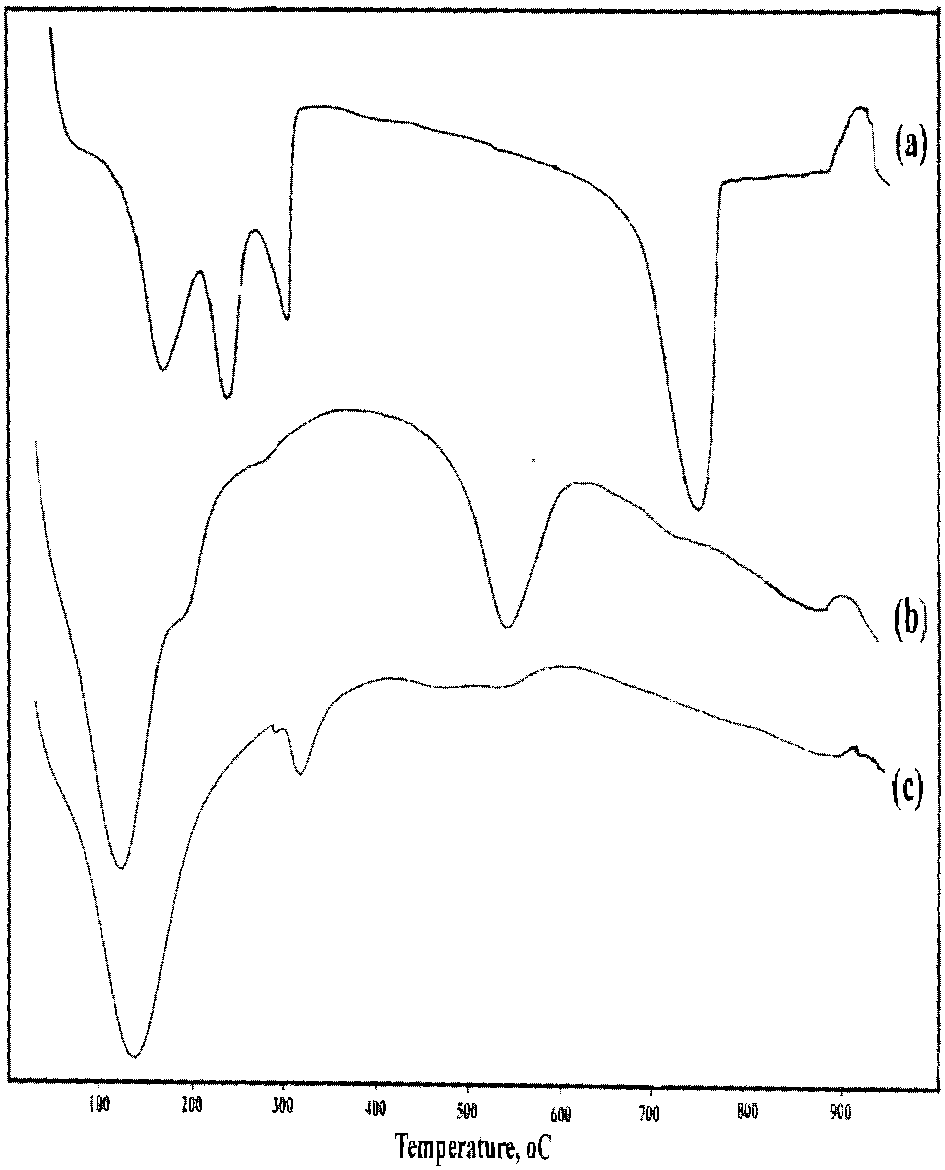

Fig (1): Differential thermal profiles of:

- **a- Sulfated zirconia.**
- **b- parent bentonite clay.**
- **c- SZPILC (10mmol SZ/gm clay).**

The DTA profile for the prepared SZ-PILC exhibits three endotherms in the range 100-300°C, the first one that results from the loss of water is broader than that for the parent clay due to strong solvation power of the Zr-polycationic species. Meanwhile, the second endotherm at 300°C can be attributed to the dehydroxylation of bulk $Zr(OH)_4$ to ZrO_4 or the substitution of terminal Zr-OH group by SO_4^{2-} **[Binghui & Gonzalez (1996)]** to form sulfated zirconia structure (Fig. 2):

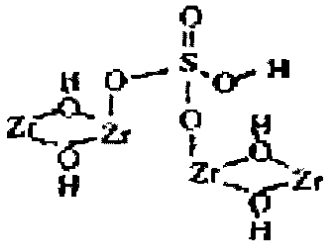

Fig. (2): sulfated zirconia structure **[Binghui & Gonzalez (1996)]**.

It is worth noting that, the broadening of the endothermic feature at ≈ 550°C (the dehydroxylation of the silicate structure) this is may be due to the cross linking of sulfated zirconia intercalated species into the interlayer hydroxyl group keeping the layer apart thereby preventing its collapse.

3.1.2 X-ray Analysis

Figure 3(a-e) shows the X-ray diffraction patterns of all the investigated samples corresponding to sulfated zirconia sample (SZ), bentonite clay, dried SZ-PILC, and SZ-PILC (Calc. I and II) respectively.

Thus the diffractogram for SZ (Fig.3-a) reveals the sample to contain a crystalline phase that corresponds to zirconium sulfate (ASTM 24-1498) and the main Characteristic lines for ZrOS (ASTM 04-0897).

The diffraction pattern for the parent clay (Fig.3-b) exhibits the main d-spacing identifying montmorillonite viz: 12.99, 4.53 &1.49Å (ASTM 12-0204), with some basal reflections for kaolinite mineral at d-values near, 7.2 & 3.33Å, in addition to quartz at, 3.36, 3.49 Å together with traces of feldspars.

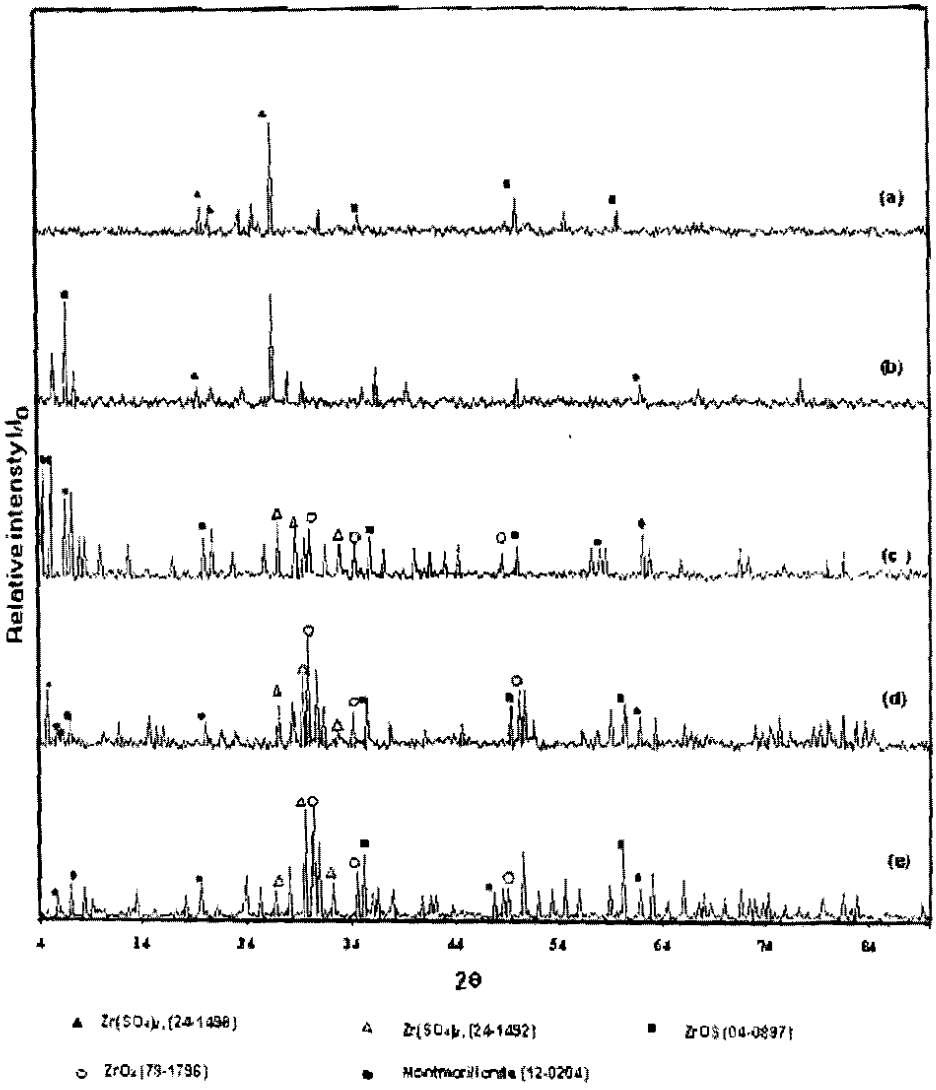

Fig (3): XRD pattren for:
a- sulfated zirconia b- Raw clay
c-Dried SZPILC d- SZ-PILC (calcined at 450°C)
e-SZ-PILC (calcined at 550° C)

For SZ-PILC (Fig.3-c), the d-spacing of montmorillonite reached 15.28, 16.75, & 19.97Å which confirm the penetration of the sulfated polycationic zirconia species into the interlamellar region, probing apart the interlayer structure resulting in the observed expansion in the interlayer distance. The creation of other d-spacings (Fig.3-c) may be attributed to the orientation of the polycationic zirconium species in the interlamella, either as a double layer of flat-lying complexes (Fig. 4), or as a single layer of complexes standing normal to the interlayer region is reasonably taking into account as stated by **[Yamanaka & Brindley (1979)]**.

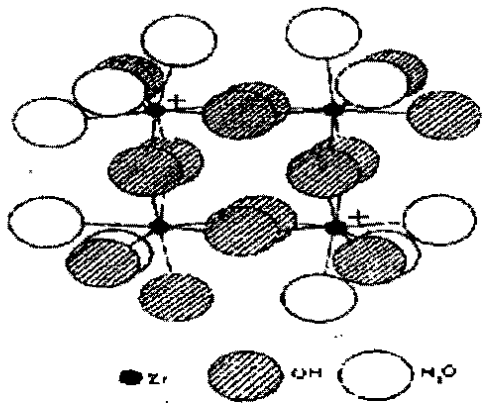

Fig. (4): Probable form of the $[Zr(OH)_{14}(H_2O)_{10}]^{2+}$ complexes **[Yamanaka & Brindley (1979)]**

Moreover, the diffractogram for SZ-PILC (Fig.3-c) reveals the presence of different characteristic lines for $Zr(SO_4)_2$ (ASTM 24-1492), (ASTM 24-1498) which may refer to the existence of different sulfated species both isolated and polynucleated in addition to the main lines for ZrOS (ASTM 04-0897) and the basal reflection for tetragonal zirconia (ASTM 79-1796).

The diffractogram for SZ-PILC (Calc.I), (Fig.3-d) exhibits some compaction in the interlayer spacing to ≈ 17.9Å instead of 19.97, due to the removal of the interlayer coordinated water molecules upon heating at 450°C. An increase in the line intensities corresponding to $Zr(SO_4)_2$, ZrOS and ZrO_2, (due to the decomposition of the polynucleated intercalated species) are observed.

For SZ-PILC calcined at 550°C there is more compaction in the interlayer gallery due to the partial dehydroxylation of the silicate

structure of the prepared PILC as clarified from the diffraction pattern (Fig.3-e).

3.1.3 FTIR Spectroscopy

Figure 5 (a-e) shows representative IR spectra for SZ, parent bentonitic clay, SZ-PILC and SZ-PILC (Calc. I and II) respectively.

The spectrum for the prepared SZ (Fig.5-a) catalyst shows two types of isolated Zr-OH groups that are in the fundamental OH stretching region located in the range 3846-3710 cm^{-1}. However, the OH bands between 3800-3700 cm^{-1} are actually assigned to the terminal OH group **[Hertl (1988)]**. The spectrum exhibits also in the OH stretching region a broad band between 3600-2850 cm^{-1} with a maximum centered at 3415 cm^{-1} which is attributed to acidic OH groups. Furthermore, characteristic sulfate bands at 1515 and 1490 cm^{-1} are assigned to asymmetric and symmetric stretching modes of sulfate groups bound via two oxygen atoms to the zirconium ion. Bands at 1092, 1154 and 1239 cm^{-1} are assigned to asymmetric and symmetric stretching modes of oxygen bound to the sulfur of sulfate **[Bensitel et al. (1988)]**.

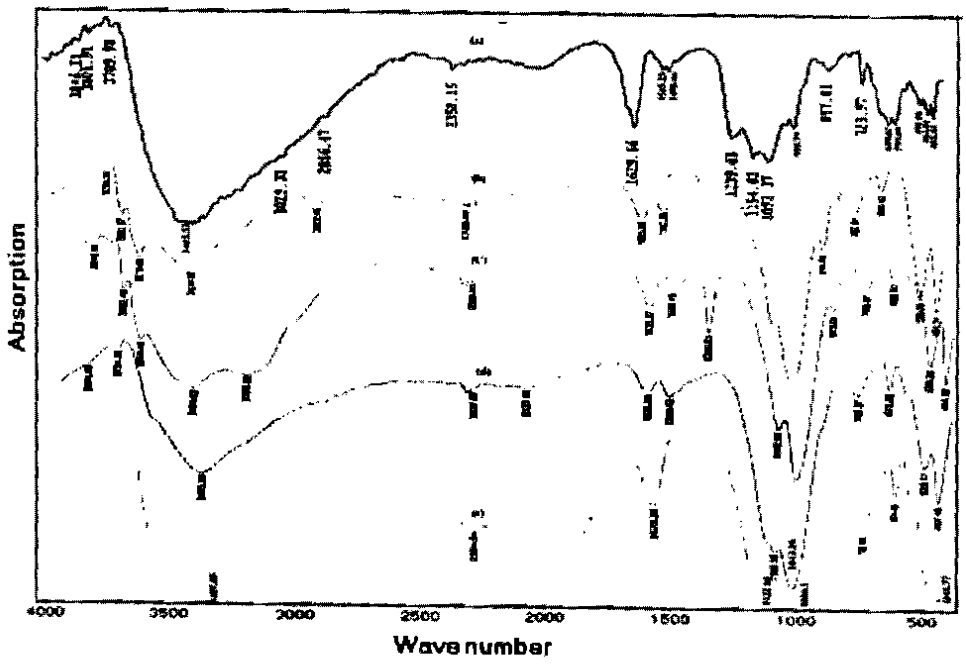

Fig (5): IR spectrum for :
a- sulfated zirconia **b- Parent clay**
c- SZ-PILC dried **d- SZ-PILC (calc. I)**
e- SZ-PILC (calc. II)

However, the mechanism of formation of covalent sulfates and poly sulfates allow us to ascribe **[Belamy (1987)]**:

- The bands concentrated at $\acute{\upsilon} < 1400$ cm^{-1} to isolated surface SO_4^{2-} groups and are postulated to be bonded to the oxide network by more than two S-O-Zr bridges **[Bensitel et al. (1988)]**.
- The bands at $\acute{\upsilon} \geq 1400$ cm^{-1} to polynuclear surface sulfates probably of the type pyrosulfates $[S_2O_7]$.
- Stretching band located at $\acute{\upsilon} \geq 1350$ cm^{-1} are ascribed to highly covalent sulfates ($\acute{\upsilon}_{S=O}$).
- Several low frequency bands at $\acute{\upsilon} \leq 1150$ cm^{-1} are due to ($\acute{\upsilon}_{S-O}$) stretching modes **[Nakamoto (1986) and Colthup et al. (1985)]**.

The spectrum for bentonite clay (Fig.5-b) reveals a large and relatively broad absorption band at OH-stretching region ranging from 3750-3400 cm^{-1} giving rise to three clear peaks at 3692, 3619 & 3414 cm^{-1} that can be assigned to the bonded and non bonded OH of the clay mineral, where the location of the OH vibrational frequencies and therefore its attachment to either the Al^{3+} octahedral or Si^{4+} tetrahedral are comparable and similar to those characterizing clay minerals. The absorption band at $\approx$ 3692 cm^{-1} is ascribed to those hydroxyl groups constituting one side of the sheet, some times referred to as inner surface hydroxyls **[Ocelli & Lester (1985)]**. The absorption band at 3619 cm^{-1} is assigned to hydroxyl groups located inside the sheet being situated at the middle layer between the tetrahedral and octahedral structures which constitute the bentonite structure **[Lahav et al. (1978)]**. The large broad band centered at $\approx$ 3415 cm^{-1} is characterized for the vibration frequencies of OH groups on the clay surface and/or on the inside of the silicate sheet structure.

The band centered at 1630 cm^{-1} is assigned to the OH vibration of the interlayer molecular water, whereas the strong band at the range 1150-920 cm^{-1} is believed to characterize bentonite being related to the OH- Al group.

Several minor absorption bands in the range of 690-920 cm^{-1} may be ascribed to the (Si-O) group of kaolinite and bentonite minerals. The two bands at the lower vibration region in the range 460-530 cm^{-1} may correspond to the vibration of Si-O groups and Si-O-Al group of kaolinite respectively.

Furthermore, the spectrum of SZ-PILC (Fig.5-c) actually reveals the main constituent bands of bentonite clay, in addition to the

appearance of relatively sharp band at ≈ 1398 cm^{-1} which is attributed to a highly covalent and/or polynuclear sulfate species (2) intercalated into the interlamellar region of the clay. Meanwhile, the small broad band at ≈ 1550 cm^{-1} may also be attributed to the existence of some isolated sulfate groups. However, an observed broadening in the OH-stretching band at ≈ 3600-3000 cm^{-1} might be attributed to the partial substitution of some OH groups of the interlayer structure by SO_4^{2-} groups or due to the crosslinking of sulfated polycationic species to the OH groups constituting the silica-silica tetrahedral sheets of bentonite.

The spectrum of SZ-PILC (Calc. I) exhibits in general, a small shift to lower frequencies and relative broadening of most bands which are ascribed to the bentonite structure 1043, 1110 & 3700-3400cm^{-1} as well as the disappearance of the characteristic band for polynucleated sulfate species at 1398cm^{-1}. This behavior can be attributed to the slight compaction in the interlayer spacing accompany the partial removal of the interlayer water [broadening of the band at 1630cm^{-1}]as well as the probable decomposition of sulfated intercalated species to smaller aggregates of sulfated zirconium species.

Further calcination to 550°C reveals partial collapse for the lamellar region due to dehydroxylation of the montmorillontic silicate structure indicated by over broadening of the OH stretching region (3692, 3620 cm^{-1} and 110 cm^{-1}), and the removal of intermolecular water (disappearance of band at 1629cm^{-1}). Moreover a relatively strong band at 1635 cm^{-1} due to isolated sulfates is also detected.

3.1.4 Textural Characteristics:

The surface texture properties of the samples have been assessed from nitrogen adsorption isotherms at -196°C. All the samples displayed type II (Fig.6-I) in the IUPAC classification **[Sing et al. (1985)]** indicating the absence of micropores.

The curves indicate that all samples have mesoporous character with a rather small hystersis loop of H_3 type closing at P/P_o 0.4-0.5 denoting the presence of aggregate of plate like particles giving rise to slit-shaped pores **[Lecloux & Pirared (1979)]**. The specific surface area values, as determined by the BET method were 108.6, 61.03 and 22.2m^2/g for the parent clay, calc I & calc II respectively. The mesoporosity is further confirmed from v-t plots (Fig.6-II) which lead in all cases to straight lines passing through the origin with upward

deviation at t = 5 in consistent with the closure point in th isotherms at P/P0 ~ 0.4.

The S_{BET} values, together with the total pore volumes and average pores diameter are summarized in Table (1). The values of average pore diameter (pore width) 28, 33 & 76.8Å indicate also the range of pore sizes assigned to mesoporosity. However, the marked increase in the average pore diameter (parent clay, calc I and calc II respectively) and consequently the significant decrease in the specific surface area is most probably due to the penetration of sulfated zirconia pillars into the porous structure of the interlamellar region that gives rise to widening of the pores. Furthermore, the decrease in the total pores volume is actually attributed to the occupation of the pores by the pillar species (sulfated zirconia species) **[Parvulescu et al. (1999)]**.

Table (1): Textural properties of the prepared samples.

Sample	S_{BET}, m^2/g	V_p, cc/g	Pore width, Å
Parent clay	108.6	0.15	28.0
SZ-PILC I	61.03	0.1	33.0
SZ-PILC II	22.2	0.08	76.8

Pore size distribution data (PSD) (Fig.6-III) reveals a major contribution by pores with an average diameter of 28, 33, 45 & 55 Å for all samples. However, the PSD curves for the samples "calc I & II" are broader and shifted slightly to larger pore sizes with significantly smaller pore fraction (dV/dD) comparing with the parent clay sample; such behavior indicates the widening of the already existed pore of the parent clay as a result of the penetration of the pillaring species and their occupation for a large fraction of pores.

3.2. Catalytic Activity

The catalytic activity of the prepared SZ and SZ-PILC catalyst is examined through n-hexane transformation reaction at temperatures varying between 180- 300°C. Data are included in Tables (2&3) and illustrated graphically in Figures 7-10.

The data indicates the typical dependence of n-hexane conversion on the reaction temperature over both catalysts, thus, increase in reaction temperature increases the total conversion (Figs.7, 8). On SZ catalyst the product distribution of n-hexane conversion reveals that methylpentane

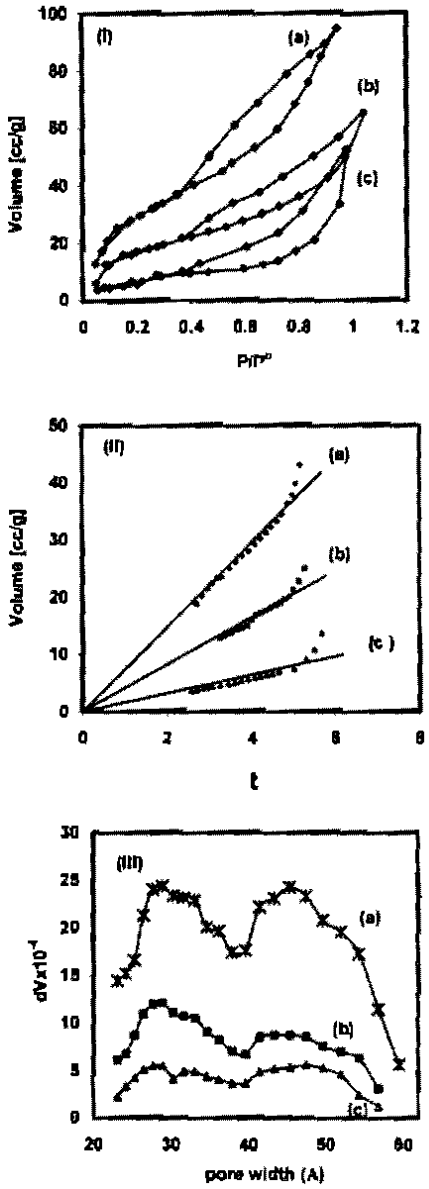

Fig(6):
I- N2 adsorption desorption isotherms of:
a- parent clay b- SZ-PILC calc. I c- SZ-PILC calc. II
II- t-plot for:
a- parent clay b- SZ-PILC calc. I c- SZ-PILC calc. II
III-PSD curves for:
a- parent clay b- SZ-PILC calc. I c- SZ-PILC calc. II

Table (2): Effect of reaction temperatures on the conversion of n-hexane over sulfated zirconia catalyst.

Reaction temperature						
	180	200	225	250	275	300
Total conversion %	18.39	21.68	22.59	25.85	27.61	29.29
Product distrbution:						
isomerization prouduct						
i-C_6	7.13	6.01	5.44	4.89	4.26	3.76
i-C7	0.24	0.41	0.60	0.79	1.07	1.13
i-C8	0.20	0.35	0.45	1.25	1.43	1.58
disporportionation products						
i-C4	4.80	8.00	9.14	11.73	13.87	16.29
i-C5	1.20	2.00	2.40	3.60	3.87	4.10
cyclic prouduct						
MCP	0.13	0.18	0.24	0.35	0.19	0.12
cracked product						
C1	0.80	0.82	0.84	0.89	0.90	0.93
C2	0.84	1.85	1.93	1.16	1.05	0.57
C3	3.00	1.95	1.40	0.98	0.71	0.51
C4	0.03	0.06	0.09	0.08	0.07	0.05
C5	0.03	0.05	0.07	0.13	0.19	0.25
Selectivity						
isomerization prouduct						
i-C_6	38.76	27.73	24.08	18.91	15.43	12.84
i-C7	1.30	1.89	2.66	3.06	3.88	3.86
i-C8	1.09	1.61	1.97	4.84	5.18	5.40
disporportionation products						
i-C4	26.10	36.91	40.47	45.37	50.24	55.62
i-C5	6.52	9.23	10.63	13.92	14.02	14.00
cyclic prouduct						
MCP	0.71	0.83	1.06	1.35	0.69	0.41
cracked product						
C1	4.35	3.76	3.72	3.44	3.26	3.18
C2	4.57	8.53	8.54	4.50	3.80	1.93
C3	16.31	9.00	6.20	3.79	2.57	1.74
C4	0.15	0.29	0.38	0.31	0.25	0.17
C5	0.14	0.23	0.29	0.50	0.69	0.85

Table (3): Effect of reaction temperature on the conversion of n-hexane over SZ-PILC calc.I.

Reaction Temperature, °C						
	180	200	225	250	275	300
Total conversion %	46.52	56.14	59.62	68.05	73.26	77.61
Product distrbution:						
Isomerization products						
methyl pentane	14.40	13.00	10.40	9.10	8.60	8.00
Dimethyl butane	5.30	4.60	4.10	3.80	3.10	2.70
Disporportionation products						
isobutane	5.3	7.6	8.1	9.8	11.5	12.7
isopentane	13.60	17.00	20.10	24.80	26.80	28.40
C7	0.95	2.20	2.45	3.40	3.70	3.96
C8	0.43	0.90	1.10	1.20	0.90	0.70
Cyclic						
methyl cyclo-pentane	1.30	2.16	2.40	2.85	3.30	3.79
Cyclo-hexane	2.20	1.86	1.63	1.01	0.93	0.62
Aromatics						
benzene	0.33	0.71	0.76	0.81	0.95	1.20
toluene	0.46	1.60	1.95	2.39	2.25	2.10
Cracked Products						
methane	0.10	0.37	1.35	1.90	2.40	3.20
ethane	0.31	0.65	0.87	1.20	1.99	2.35
propene	0.16	0.29	0.40	0.80	0.86	0.89
propane	0.41	0.77	0.92	1.20	1.50	1.80
butane	0.69	1.58	1.75	1.89	1.98	2.00
pentane	0.58	0.85	1.34	1.90	2.50	3.20
Selectivity %						
Isomerization products						
methyl pentane	30.95	23.16	17.44	13.37	11.74	10.31
Dimethyl butane	11.39	8.19	6.88	5.58	4.23	3.48
Disporportionation products						
isobutane	11.39	13.54	13.59	14.40	15.70	16.36
isopentane	29.23	30.28	33.71	36.44	36.58	36.59
C7	2.04	3.92	4.11	5.00	5.05	5.10
C8	0.92	1.60	1.85	1.76	1.23	0.90
Cyclic						
methyl cyclo-pentane	2.80	3.85	4.03	4.19	4.50	4.88
Cyclo-hexane	4.73	3.31	2.73	1.48	1.27	0.80
Aromatics						
benzene	0.71	1.27	1.27	1.20	1.30	1.55
toiuene	1.10	0.91	0.78	0.83	0.51	0.50
Cracked Products						
methane	0.22	0.65	2.26	2.79	3.28	4.12
ethane	0.66	1.16	1.46	1.76	2.72	3.03
propene	0.34	0.52	0.67	1.18	1.17	1.15
propane	0.88	1.37	1.54	1.76	2.05	2.32
butane	1.48	2.81	2.94	2.78	2.70	2.58
pentane	1.25	1.51	2.25	2.79	3.41	4.12

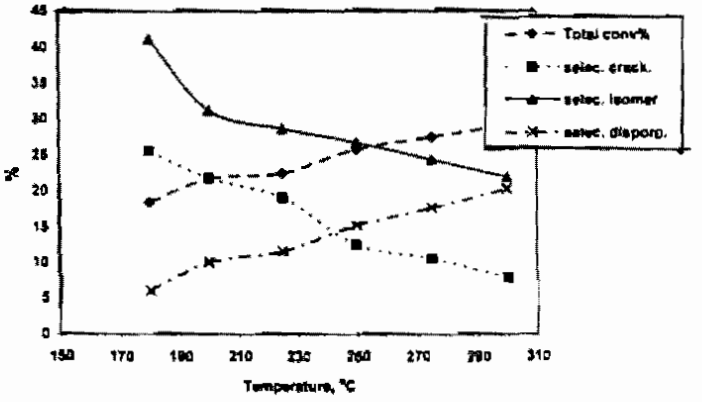

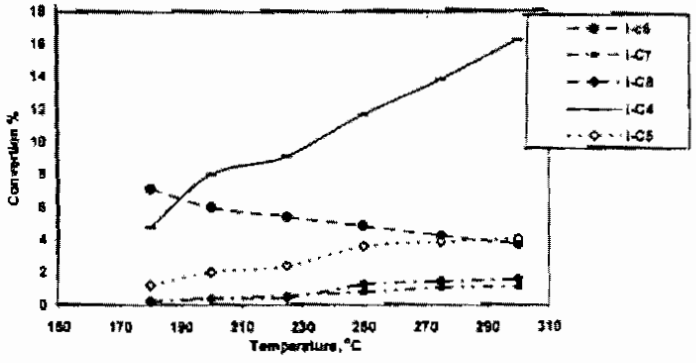

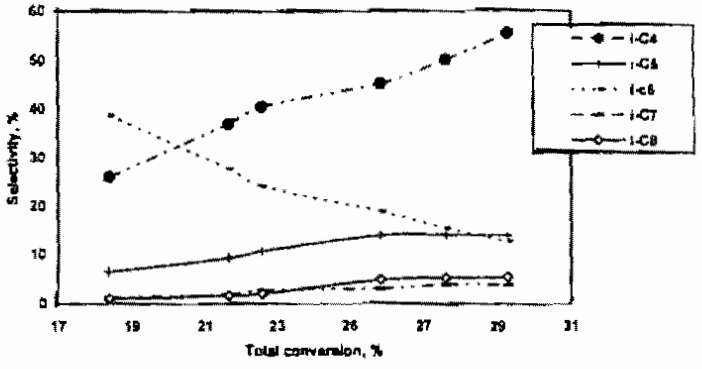

Fig. 7: Product distribution of n-hexane over SZ

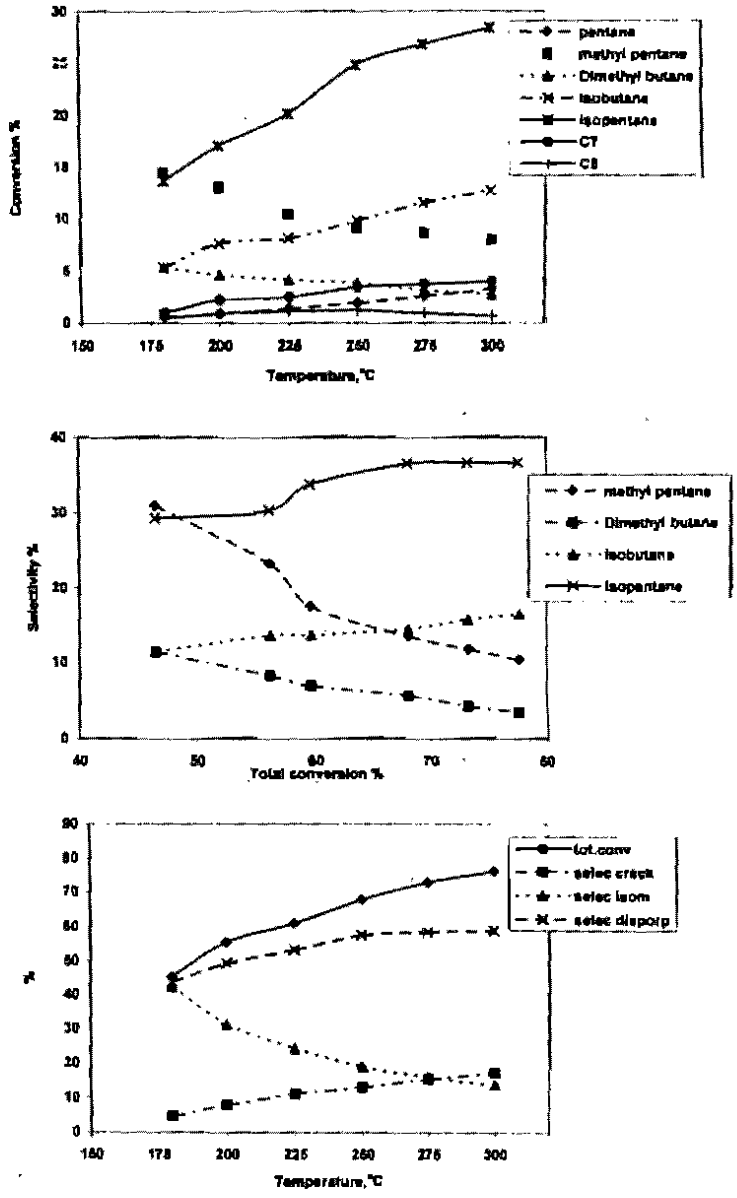

Fig 5: Product distribution of n-hexane over SZ-PILC

(iso-hexane) is the predominate isomeric product. Whereas, its selectivity decreases gradually with the increase in the total conversion. On the other hand iso-butane is considered as the main product at all reaction temperatures, its selectivity increases with the total conversion. Considerable amount of isopentane is also obtained with incremental selectivity with the increase in the total conversion (Fig.7). Propane, ethane and methane were within detection limits. Skeletal isomers (i-C_7 & i-C_8) were among the minor products with selectivities $\leq$ 5% at the highest total conversion.

The conversion of n-hexane over SZ-PILC seems to follow the same trend as SZ (histogramatically in fig 9&10). Product distribution of n-hexane conversion over SZ-PILC (Table 3) reveals that, two main isomeric products for n-hexane are obtained, monobranched isomer (methyl pentane) and dibranched isomer (dimethyl butane) which decrease with the increase in reaction temperature. Their selectivity exhibit a gradual decrease with an increase in the total conversion. The sharp decrease of these isomeric products at reaction temperatures over 200 ^{o}C. is a result of the consecutive cracking reactions (Fig. 8) and is accompanied by a marked increase in the yield of iso-pentane and iso-butane.

Moreover, the significant amounts of C_6^+ products (C_7 &C_8) that increase with the total conversion (Table 3), may be related to a disproportionation reaction **[Cheung & Gates (1997) and Rezgu & Gates (1996)]**. Methylcyclopentane, cyclohexane, benzene and toluene are also formed. The formation of these cyclic products may take place via either a selective or a non-selective dehydrocyclization process of n-hexane which corresponds to the reverse reaction of a selective or non selective cyclic mechanism **[Paal (1980) and Gault (1982)]**. Furthermore, cyclohexane may undergo dehydrogenation leading to the production of benzene and 1-5 ring contraction that giving rise to methyl cyclopentane which occurs on acidic sites **[Gault (1989)]**. Thus the reaction network of n-hexane conversion over the prepared catalysts can be represented in the following scheme 1:

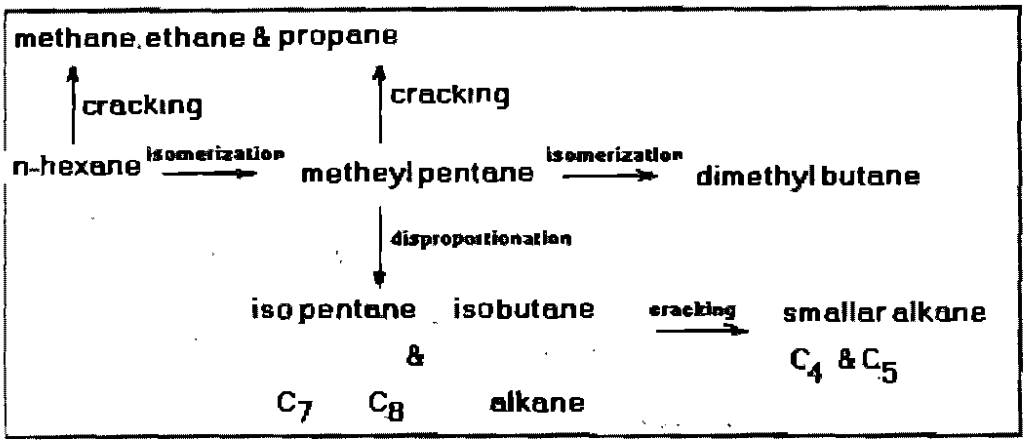

Scheme (1)

The reactions shown in the scheme are generally believed to proceed via carbenium ions, however, the high abundance of iso-pentane and iso-butane may indicate the high preferance of bimolecular reactions **[Garin (1991); Iglesia et al. (1993) and Sayaria (1997)]**. One of the possible routes would involve splitting at the center of a n-hexane molecule to give a surface C_3 entity. This may not desorb as propane but seems to react with another C_6 unit to form a C_9 intermediate that produces iso-pentane and iso-putane **[Haag & Dessau (1984) and Bouchenafa-saib et al. (2004)]**.

Thus, the product distribution data are consistent with acid-base catalysis, whereby isomerization, disproportionation, and cracking take place via carbinium ion mechanism **[Ryu & Gates (1998)]**.

Consistent with this pattern, one would speculate the isomerization process to proceed via monomolecular mechanism that predominates initially followed by bimolecular mechanism that results in disproportionation and izomerization processes. This speculative suggestion is consistent with the evidence of direct cracking of n-hexane to give methane, ethane and propane which might involve the protonation of n-hexane reactant by the catalyst.

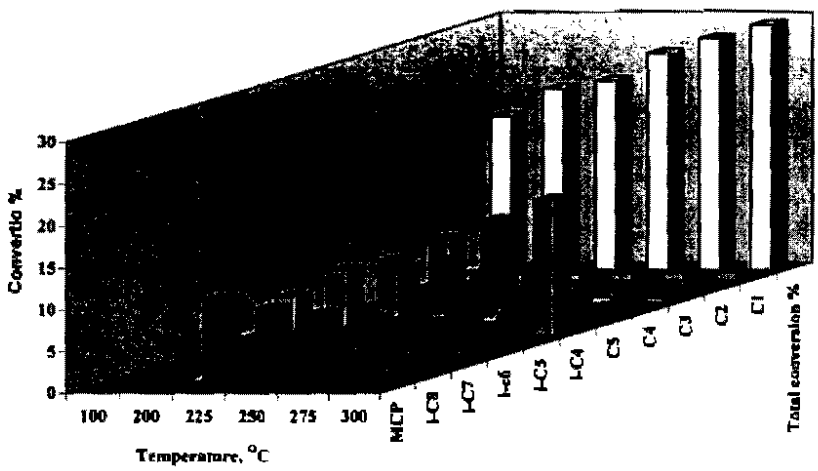

Fig. (9): Product distribution of n-hexane conversion over sulfated zirconia catalyst

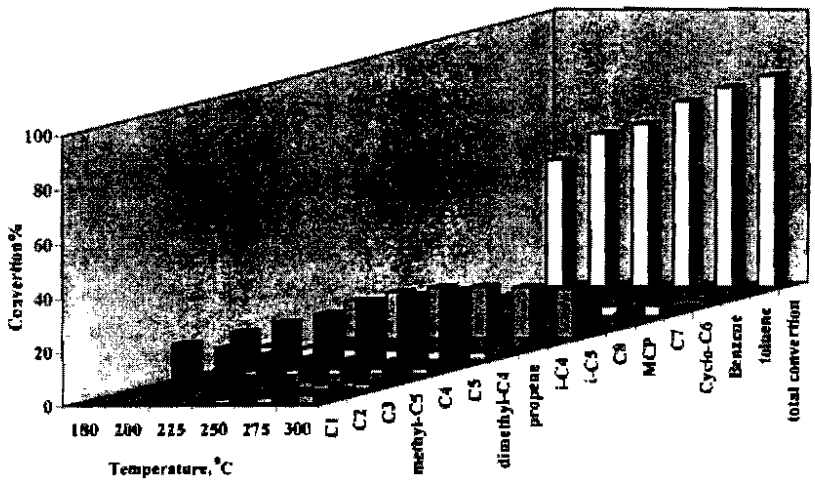

Fig. (10): Product distribution of n-hexane conversion over sulfated zirconia pillared clay (450)

4. CONCLUSION

The results presented in this work show that sulfated zirconium modified pillared clay can be obtained with good thermal stability and modified structural and textural properties. The results also indicate that SZ-PILC shows inferior performance in n-hexane transformation via isomerization, disproportionation and cracking reactions. The n-hexane isomerization takes place predominantly at the lower temperatures, whereas disproportionation becomes predominant at the higher temperatures. The higher isomerization activity and selectivity of the modified sulfated zirconia pillared clay, even at lower temperatures, is inferred to acidity enhancement by the effect of sulfate groups. SZ-PILC catalyst is also active for the formation of dibranched product under the present experimental conditions, which implies that they meet the demanding criteria for production of higher octane number alkanes.

REFERENCES

Barshad, I.: Am. Miner. 35, (1950) 225.

Bellamy, L. J. "The Infrared of Complex Molecules", Chapman and Hall, London, 1987.

Ben Chaabene, S. Bergaoui, L. Ghorbel, A. Lambert, J.-F. Stud. Surf. Sci. Catal. 143 (2002) 1053.

Bensitel, M. Saur, O. Lavalley, J. C. and Morrow, B. A. Mater. Chem. Phys. 19, (1988) 147.

Bergaoui, L. Ghorbel, A, Lambert, J.-F. Stud. Surf. Sci. Catal. 142 (2002) 903.

Binghui, L. and Gonzalez, R. D. Ind. Eng. Chem. Res., 35, (1996) 3141.

Bouchenafa-Saib, N. Issaadi, R. Grange, P. Applied Catalysis 259 (2004)9.

Cheung, T. K. Gates, B. C. A. J. Catal., 168, (1997) 522.

Colthup, N. B. Daly, L. H. and Wiberley, S. E. "Introduction to Infrared and Raman Spectroscopy", P. 353, Acadimic Press, New York, 1975.

Farfan-Torres, E. M. Grange, P. Catal. Sci. Technol. 1 (1991) 103.

Farfan-Torres, E. M. Grange, P. C. R. Acad. Sci. Belg. 4/5 (1990) 113.

Farfan-Torres, E. M. Sham, E. Grange, P. Catal. Today 15 (1992) 515.

Garin, F. Maire, G. Acc. Chem. Res. 22 (1989) 100.

Garin, F. Andriamasinoro, Abdulamad, Sommer, A. J. Catal. 131 (1991) 199.

Gault, F. G. Adv. Catal., 30 (1982) 267.

Haag, W.O. Dessau, R. M. in: Proceedings of the 8th international congress on catal.,Berlin (West), Vol. 2, Verlag Chemie, Weinheim, 1984, p 305.

Hertl, W. langmuir 5, (1988), 96.

Iglesia, E. Soled, S. L. Kramer, G. M. J. Catal, 144. (1993) 238.

Issaadi, F.o.Garin, R. et al., Catalysis Today 113(2006) 166.

Katoh, M. Fujisawa, H. Yamaguchi, T. Stud. Surf. Sci. Catal. 90 (1994) 263.

Lahav, N. Shani, U. and Shabtai, J. Clays clay mineral, 26 (1978) 107.

Lambert, J. F. Poncelet, G. Top. Catal. 4(1997)43.

Lecloux, A. Pirared, J. P. J. Colloid Interface Sci., 70, 265 (1979).

Nakamoto, K. 'Infrared and Raman Spectra of inorganic and Coordination Compounds", P.249, Wiley-Interscience, New York, 1986.

Ocelli, M. L. Lester, J. E. Ind. Eng. Chem. Prod. Res. Dev. 24, (1985) 27.

Paal, Z. Adv. Catal., 29 (1980) 273.

Parvulescu, V. Coman, S. Grange, P. Parvulescu, V. I. Apple. Catal. A: General 176, (1999) 27.

Rezgu, Gates, B. C., Catal. Lett., 37, (1996) 5.

Ryu, S. G. Gates, B. C. Ind. Eng. Chem., Res., 37, (1998), 786.

Sayaria, A. Yang, Y. Song, X. J. Catal. 167 (1997) 346.

Sing, K. S. W. Everett, D. H. Haul, R. A. W. Moscou, L. Pierotti, R. A. J. Rouquerol, T. Siemieniewska, Pure Appl. Chem. 57 (1985) 603.

Srinivasan R. et al. : Applied Catalysis 130 (1995) 135.

Vaughan, D. E. W Catal. Today 2(1988) 187.

Verà, C.R. Appl. Catal. A: General 230(2002) 137.

Yamanaka S. and Brindley, W. Clay and Clay Mineral, 27, (1979), 119.

Yamanaka, S. and Brindley, G. W. Clay and Clay Minerals, 27, (1979) 119. Watkins,R. Srinivasan, C. Hubbard, B. H., Davis, Chem. Mater. 7, (1995) 725.

الحفازات ذات الشكل الأسطوانى المعدله بواسطة كبريتات الزركونيا وتوصيفها كعامل حفاز فى تحويل الهكسان

داليا رضوان- لمياء سعد- سارة ميخائيل - سوزى الفونس سليم

تضمن هذا البحث تحضير الحفازات ذات الشكل الأسطوانى المعدله بواسطة كبريتات الزركونيا عن طريق أضافة الكبريتات الى الزركونيا قبل عملية ال (pillaring). وقد تم تتبع التغير التركيبى للمواد المحضرة بأستخدام طرق التوصيف المختلفة مثل حيود الأشعة السينية (XRD)، التغيرات الناتجة عن المعاملات الحرارية (DTA & TGA) التغير فى المساحة السطحية والمسامية (BET)، كذلك تم أستخدام الأشعه فوق الحمراء (I.R) لتتبع التغير فى المجموعات الوظيفيه. وقد أثبتت الدراسة حدوث تغيرات إيجابية فى تركيب المواد المحضرة بعد عملية ال pillaring بواسطة كبريتات الزركونيا بما يفيد أستخدامها فى تفاعلات الهكسان المختلفة وخاصة تفاعل الأزمره isomerization .